THE JOURNAL OF PHYSICAL CHEMISTRY A

Article

Cite This: J. Phys. Chem. A 2017, 121, 8791-8798

pubs.acs.org/JPCA

ReaxFF Reactive Molecular Dynamics Study of Orientation Dependence of Initial Silicon Carbide Oxidation

Vito Šimonka,[†] Andreas Hössinger,[§] Josef Weinbub,*[,†] and Siegfried Selberherr[‡]

[†]Christian Doppler Laboratory for High Performance TCAD, Institute for Microelectronics, and [‡]Institute for Microelectronics, TU Wien, Gußhausstraße 27-29/E360, 1040 Wien, Austria

[§]Silvaco Europe Ltd., Compass Point, St. Ives, Cambridge PE27 5JL, United Kingdom

Supporting Information

ABSTRACT: We analyze the early stage of the highly anisotropic silicon carbide oxidation behavior with reactive force field molecular dynamics simulations. The oxidation of a-, C,- m-, and Si-crystallographic faces is studied at typical industry-focused temperatures in the range from 900 to 1200 °C based on the time evolution of the oxidation mechanism. The oxide thicknesses and the growth rates are obtained from these simulation results. In addition, an investigation of the silicon and carbon emission is performed with respect to various orientations in order to support further development of macroscopic physical models that aim to predict initial silicon carbide oxidation.

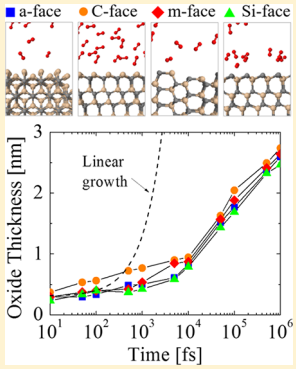

INTRODUCTION

One of the key fabrication steps in semiconductor industries is thermal oxidation. The oxidation process produces a thin layer of oxide, usually silicon dioxide (SiO_2), which is used as a high-quality insulating layer, a part of the gate in a metal−oxide−semiconductor field-effect transistor (MOSFET), or a mask for ion implantation in various electronic devices.[1] Semiconductor materials like silicon (Si) and silicon carbide (SiC) are due to the ability of forming high quality oxides, among the dominating materials for fabricating integrated circuits. Recent studies have shown a considerable potential for SiC-based devices for high temperature and high voltage electronics due to the properties of SiC, including a wide band bap, a high breakdown field, and a high thermal conductivity.[2] These properties are particularly attractive for power devices with low power loss.[3] In addition, SiC is highly resistant to radiation and other extreme environments and is thus also attractive for applications in aerospace and nuclear plants.[4,5]

However, there are still many issues to be solved on the material level, and the governing theory is not as mature as, for instance, for Si, e.g., electrical activation of impurities,[6,7] SiC/SiO_2 interface defects,[8] and orientation-dependent oxidation.[9−11] These shortcomings require analyses on the microscopic levels, which will lead to performance improvements of SiC devices, e.g., inversion channel mobility[12] and gate oxide stability,[13] in order to further reduce the on-resistance and enhance the gate reliability.[3] In particular, a detailed understanding of the atomic and molecular interactions of oxygen (O) and SiC will enable advances in SiC oxidation processes and thus assist in the goal of maximizing the efficiency of SiC devices and the corresponding device manufacturing processes.[14,15]

SiC has over 250 polytypes, among which the most popular for device manufacturing are 3C, 6H, and 4H due to their attractive physical properties. The variations of the polytypes are identical in two dimensions but differ in the third and can be viewed as layers stacked in a certain sequence. The electronic properties as well as physical reaction mechanisms vary with the stacking sequence of the SiC layers, forming either a cubic, a hexagonal, or a rhombohedral crystal structure. In this study we focus on 4H-SiC, which is currently the preferred polytype for power electronics due to the advances in 4H growth technology and its attractive electronic properties,[3] i.e., the largest band bap and the highest carrier mobility among the polytypes.[16] 4H-SiC has a hexagonal structure and the stacking sequence ABAC, shown in Figure 1a.

Thermal oxidation of SiC is compared to the oxidation of Si, a considerably more complicated process due to the addition of the carbon species. It is commonly represented with the chemical formula $SiC + {}^3/_2O_2 \rightarrow SiO_2 + CO$. In addition, the reaction rates of the SiC oxidation depend highly on the crystal orientation. In particular, the most diverse oxidation rates have been reported for the four common faces:[17−19] a $(11\bar{2}0)$, C $(000\bar{1})$, m $(1\bar{1}00)$, and Si (0001), shown in Figure 1b. The inevitable orientation dependence has significant consequences for nonplanar device structures[20] and requires an advanced

Received: September 8, 2017
Revised: October 30, 2017
Published: October 31, 2017

DOI: 10.1021/acs.jpca.7b08983
J. Phys. Chem. A 2017, 121, 8791−8798

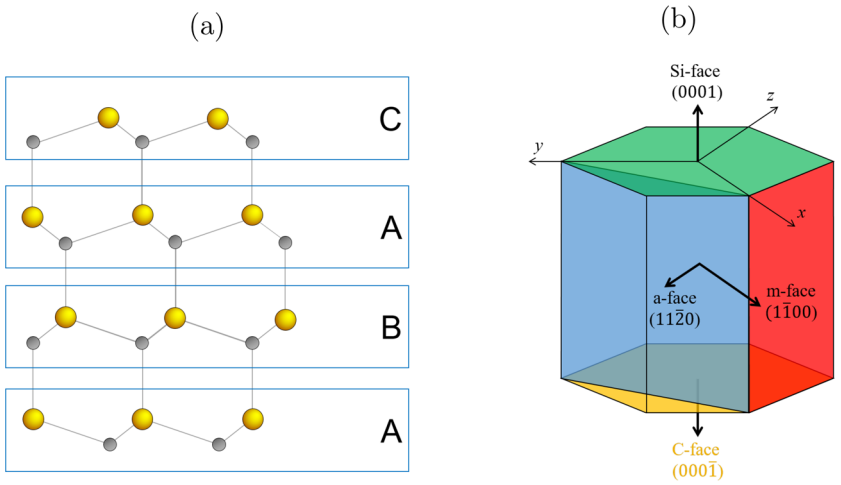

Figure 1. (a) Cross section of a basic cell of 4H-SiC with the stacking sequence ABAC. (b) Schematic representation of the four common faces. Yellow and gray spheres represent Si and C, respectively. The green hexagon represents Si-, the yellow hexagon C-, the blue square a-, and the red square m-face.

high-accuracy modeling approach to correctly predict the oxide formation for the overall device.[11]

The established macroscopic oxidation model for Si is the Deal Grove model,[21] which has introduced the relationship between the oxide thickness (X) and the oxidation time (t). The Deal Grove model has also been applied in a modified form for the oxidation of SiC.[22] However, the oxidation growth cannot be described properly with the Deal Grove model in the entire thickness region due to the rapid rate decrease in the initial oxidation stage for both Si[23,24] and SiC.[25−28] In order to empirically represent the oxidation growth rates below an oxide thickness of a few tens of nanometers, Massoud's empirical relation[23,24] has been proposed. Those empirical models showed success in reproducing the growth rate data for SiC oxidation.[9,11,29] However, the model in this state lacks an important SiC orientation-based feature, which has been recently proposed in order to augment three-dimensional SiC process simulations.[7,11] Moreover, the exponential term of Massoud's empirical relation is not based on physical considerations, but only on fitting experimental results. To overcome this shortcoming, a Si and C emission model[28] has been proposed based on the interfacial Si and C emission phenomenon.[30] This model introduces Si and C emission into the oxide, which reduce the interfacial reaction rate.[14] However, the growth rate data are restricted to the Si-, C-, and a-face. Therefore, the orientation-dependent oxidation mechanism of SiC cannot yet be fully validated with experiments.

The initial oxidation process of SiC has been also studied based on molecular-level simulations, which have been performed for up to 100 ps at various temperatures in the range 500−5000 K.[31] Newsome et al. have in this way expanded molecular-level simulations to investigate the early stage of the SiC oxidation, which lead to an accurate analysis of bond formations. This approach enables investigations of the early stages of the oxidation process, where the experimental methods fail to provide the necessary data due to technical issues to accurately measure the oxide growth on very short time scales. However, the orientation-dependent investigation of the initial oxidation process, which is essential to further develop macroscopic physical models incorporating SiC anisotropy, is currently missing.

The focus of this study is therefore to perform molecular-level simulations of the initial SiC oxidation process with respect to various crystal orientations, including the a-, C-, m-, and Si-face of 4H-SiC, and typical oxidation temperatures in the range 900−1200 °C. We investigate the time evolution of the oxidation process and extract the growth of the oxide via the number of bonded O molecules in the SiC crystal as well as the number of emitted Si and C interstitials. These investigations provide the basis to further develop macroscopic models, which are critical to research and industry to further push the capabilities of future SiC devices.

COMPUTATIONAL METHODS

Computational methods on atomic or molecular levels provide powerful ways to explore, develop, and optimize novel materials. Such methods, commonly based on quantum mechanics (QM),[32] are computationally very expensive and can thus be applied only to small-sized atomic systems, typically containing a few tens of atoms. To overcome this issue, QM structure and energy data can be used to train empirical force fields in order to reduce the demand on computational resources.[31] In this work, we use a novel empirical ReaxFF reactive force-field method.[33,34] This method replaces harmonic bonds of conventional molecular dynamics (MD) with bond orders and energies that depend on interatomic distances, which thus reduces simulation time by several orders of magnitude.[35−38]

The parameters involved in the ReaxFF potential functions must be parametrized against high-level *ab initio* calculations and experimental results. We use the ReaxFF potentials by Newsome et al.[31] and Kulkarni et al.,[39] which were particularly developed for the atoms involved in the SiC oxidation, i.e., Si/C/O.[40] All of the simulations are performed with both ReaxFF potentials in parallel to ensure maximal accuracy and robustness of results.

State-of-the-art implementations of ReaxFF, e.g., PuReMD[41] and LAMMPS,[42] have demonstrated good computational efficiency and accuracy. We use LAMMPS, which is distributed as an open-source code and supports parallel computing via OpenMP and MPI.

DOI: 10.1021/acs.jpca.7b08983
J. Phys. Chem. A 2017, 121, 8791−8798

SIMULATION SETUP

Our goal was to treat several layers of SiO_2 reflecting differences between various SiC orientations. Therefore, we have simulated 1 ns oxide growth with 2×10^6 time steps using a 0.5 fs time step. The number of atoms involved in the simulations must be appropriately limited in order to be able to perform the desired number of time steps. On the other hand, the number of O_2 molecules must be high enough to ensure a constant gas flow. For this reason, numerous control simulations have been performed with respect to various simulation box sizes to ensure that the product gases in the air do not further affect the oxidation and that an adequate number of O_2 molecules is available at every time step of the simulation. Our initial structure setup consists of approximately 10 SiC layers in x and y directions and 27 SiC layers in the z direction. The space on top of the substrate is 3 times the height of the crystal with randomly and uniformly distributed O_2 molecules, indicating dry air conditions for the thermal oxidation. The schematic representation of the $3 \times 3 \times 24$ nm^3 simulation box is shown in Figure 2. The total number of particles in all of the simulations was approximately 10^4, out of which ≈3600 are Si and C atoms. The surfaces of SiC were not initially passivated, as the passivated surfaces could affect the investigation of the orientation dependence of the oxidation growth rates.[43].

All simulations were performed in the canonical ensemble, depending on the absolute temperature, number of particles, and volume (NVT). Periodic boundary conditions in x and y directions and a reflective boundary in the z direction were used to avoid undesired oxidation on the bottom of the substrate. The temperature of the simulations was controlled with the Berendsen thermostat[44] with a temperature damping constant of 100 fs. We have performed simulations with four common industry-focused oxidation temperatures: T = 900, 1000, 1100, and 1200 °C. In order to investigate orientation dependence, four different initial structures were prepared, which represent the four considered SiC faces, shown in Figure 3.

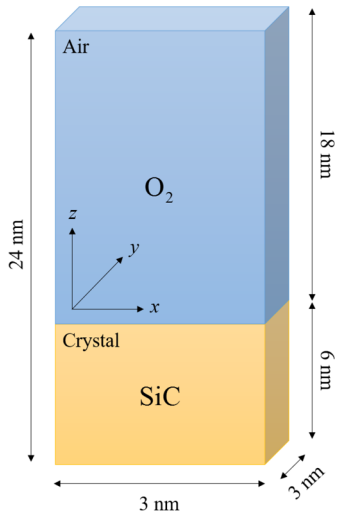

Figure 2. Schematic representation of the simulation setup. The simulation box is composed of two cuboids, namely air and crystal. The air includes only O_2 molecules and the crystal only SiC compounds.

RESULTS AND DISCUSSION

We have executed LAMMPS on the Vienna Scientific Cluster (VSC-3),[45] which consists of 2020 nodes, each equipped with two 8-core Intel Xeon E5-2650v2 2.6 GHz processors (total of 16 physical/32 logical cores per node) and 64 GB of main memory. An initial evaluation of the parallelization backends of LAMMPS (i.e., USER-OMP package, including OpenMP and MPI) showed better performance for our tasks with a pure MPI approach compared to using a hybrid MPI and OpenMP approach. Figure 4 shows a benchmark of our simulation setup

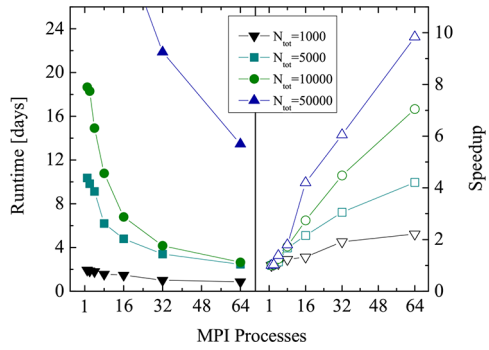

Figure 4. Runtime and speedup of pure MPI LAMMPS simulations as a function of MPI processes for various atom numbers N_{tot}. Benchmarks recorded on VSC-3 with 1 OpenMP thread and 16 MPI processes per core.

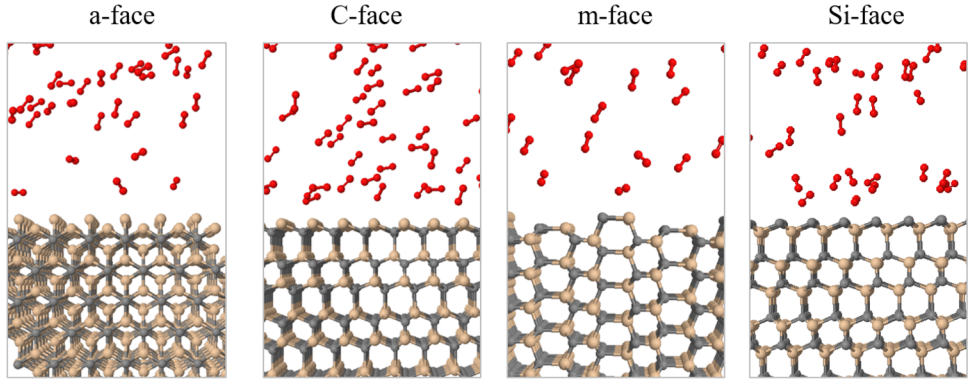

Figure 3. Simulation snapshots of initial structures of the SiC/O_2 interfaces for a- $(11\bar{2}0)$, C- $(000\bar{1})$, m- $(1\bar{1}00)$, and Si- (0001) oriented SiC at time = 0.

DOI: 10.1021/acs.jpca.7b08983
J. Phys. Chem. A 2017, 121, 8791−8798

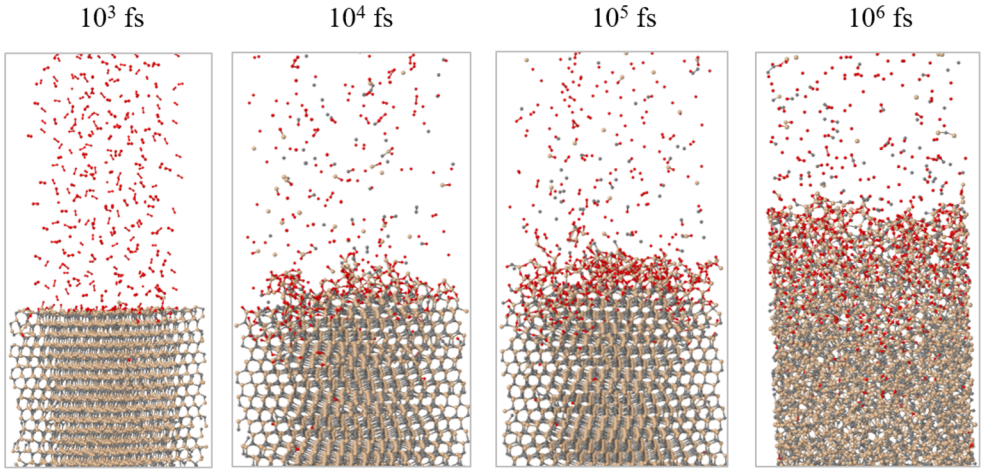

Figure 5. Simulation snapshots of the structural evolution of the SiC (0001) Si-face oxidation process for $t = 10^3$, 10^4, 10^5, and 10^6 fs at $T = 1100$ °C. The time step is 1 fs.

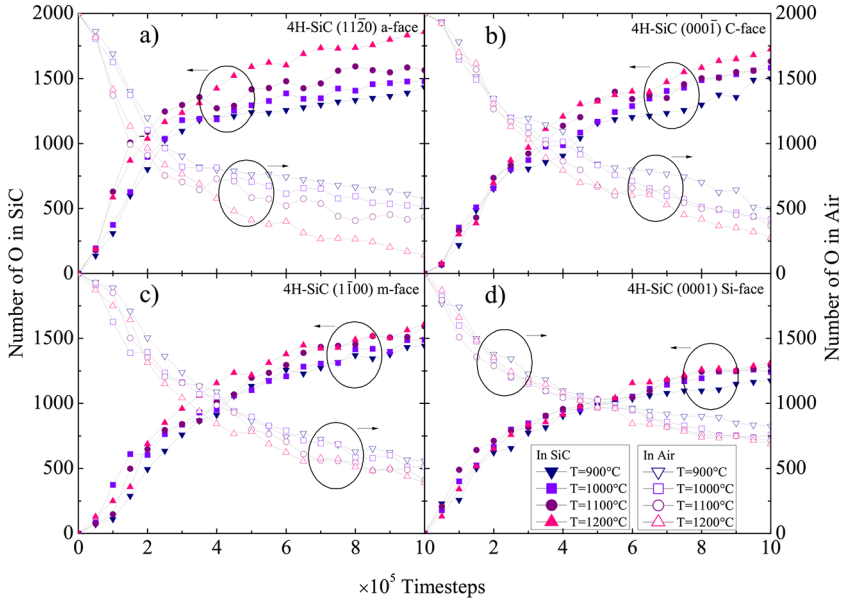

Figure 6. Time evolution of the number of O atoms in the SiC crystal (closed symbols, left axis) and in the air (open symbols, right axis) for the (a) a-, (b) C-, (c) m-, and (d) Si-face. Colors refer to various oxidation temperatures in the range from 900 to 1200 °C.

for various atom numbers and up to 64 MPI processes. Despite the relatively low parallel efficiency of our simulations (i.e., 35% in the best case), using LAMMPS' USER-OMP package enables to significantly reduce the overall simulation runtime (e.g., from 18 to 4 days for 10^4 particles).

One of the objectives of this work has been to study the transient oxidation process of SiC. The structural evolution of the SiC/O_2 system is shown in Figure 5 for 10^3, 10^4, 10^5, and 10^6 fs. The time evolution clearly shows all of the oxidation process steps: (i) transport of O_2 to the oxide surface, (ii) in-diffusion of O_2 through the oxide film, (iii) reaction of O_2 and SiC at the SiO_2/SiC interface, (iv) out-diffusion of carbon oxide (CO) through the oxide film, and (v) removal of the product gases away from the oxide surface.

To follow the oxidation process, we analyze the number of O atoms in the SiC crystal (N_O^{SiC}) and air (N_O^{Air}). The evolution of the O atoms reacting with the SiC structure for the four crystallographic faces at $T = 900$, 1000, 1100, and 1200 °C is shown in Figure 6. It is clearly evident that the concentration of the O atoms in SiC is increasing with time, which indicates a successful oxidation process. As the SiO_2 is formed on top of the crystal, the chemical reaction is passivated, which is evident by the decreasing slope of the curves. The formed oxide affects the in-diffusion of the O_2 and the out-diffusion of the product gases through the oxide film; therefore, the oxidation process is decelerated.

Another essential figure of merit is the time evolution of the number of Si (N_{Si}^{SiC}) and C (N_C^{SiC}) atoms in the SiC crystal. The results for the four SiC faces and for the four investigated temperatures are shown in Figure 7. Si and C in this case are traced as single atoms but are in fact diffused out of the crystal as product gases. The oxidation temperature clearly affects the diffusion of the Si, C, and O species, which confirms that even the early stage of the oxidation mechanism, i.e., <1 ns, is temperature-dependent. The figures additionally suggest that the out-diffusion of the C interstitials is higher than Si interstitials. This is in agreement with previous reports[28] and confirms the assumption of the Si and C emission model[14,16]

DOI: 10.1021/acs.jpca.7b08983
J. Phys. Chem. A 2017, 121, 8791−8798

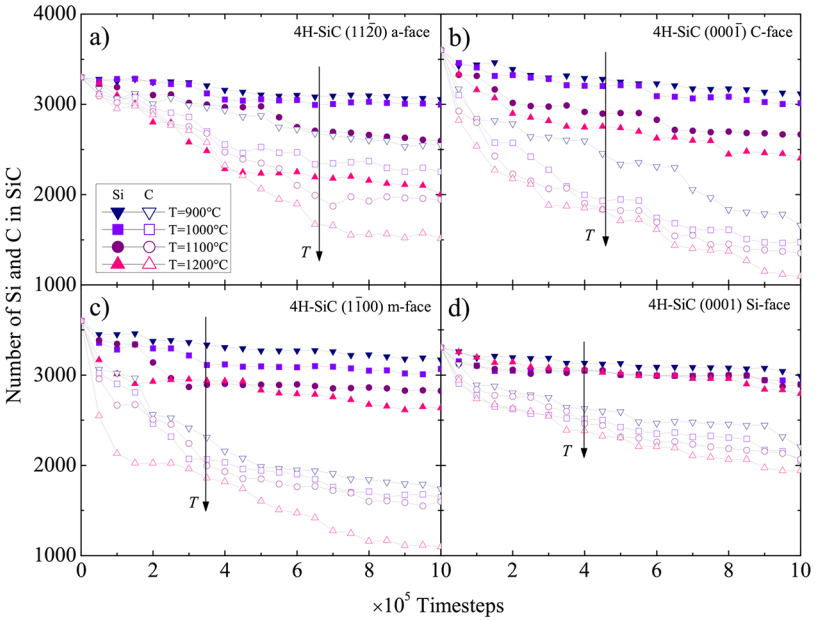

Figure 7. Time evolution of the number of Si (closed symbols) and C (open symbols) atoms in the SiC crystal for the (a) a-, (b) C-, (c) m-, and (d) Si-face. Colors refer to various oxidation temperatures in the range from 900 to 1200 °C.

that the accumulation of the C interstitials becomes saturated prior to that of the Si interstitials. In addition, C and Si emission suppresses the interfacial reaction rate during oxidation.

We further investigated the impact of the anisotropy on the oxide thickness for the particular case of 1100 °C, as seen in Figure 8 for the four crystallographic faces. The oxide thickness

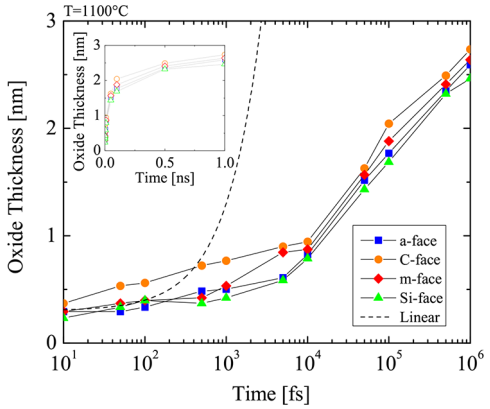

Figure 8. Time evolution of the oxide thickness for the a-, C-, m-, and Si-face at T = 1100 °C. The dashed line shows a symbolic assumption of inaccurate linear growth of the SiO_2 thickness. The inset figure uses a linear x-axis.

was calculated for each time step of the simulation. To obtain meaningful data points for a semilog and log−log representation, the recorded data were extracted for each 5- and 10-times multiple of the simulation time. The results show that even after a very short time of oxidation (i.e., 1 ns) the thickness of the oxide grows up to 2.5 nm. This suggest that the initial oxidation is taking place almost instantaneously relative to the industry-focused oxidation times and clarifies the assumption of the macroscopic models[9] that the oxide thickness at $t \approx 0$ is approximately 5 nm. We have plotted a symbolic linear growth rate (dashed line) with the slope of 1×10^{-3} nm/fs and the intercept 0.3 nm to highlight the difference between the simulation results and a hypothetical but inaccurate linear assumption: This clearly shows that a linear growth rate cannot be assumed. Comparing the oxide evolution with the linear growth, it is evident that the growth rate is significantly reduced as the oxide layer grows. Thus, it can be clearly seen that the relationship between the oxide thickness and the time is exponential for the early stage of the oxidation.

In addition, we have obtained and normalized the emitted Si and C species as $R_{Si} = N_{Si}^{emitted}/N_{Si}^{tot}$ and $R_C = N_C^{emitted}/N_C^{tot}$, respectively, where $N^{emitted}$ is the number of emitted and N^{tot} the total number of Si or C. The time evolution of the normalized emission and the emission rates of Si and C are shown in Figure 9. The results suggest differences between the four crystallographic faces and indicate that R_C is approximately 3 times higher than R_{Si} across the whole time scale. An unexpected peak has been observed for the emission rates between 10 and 100 ps, regardless of the crystal orientation. It appears that at times <10 ps the oxidation mechanism does not

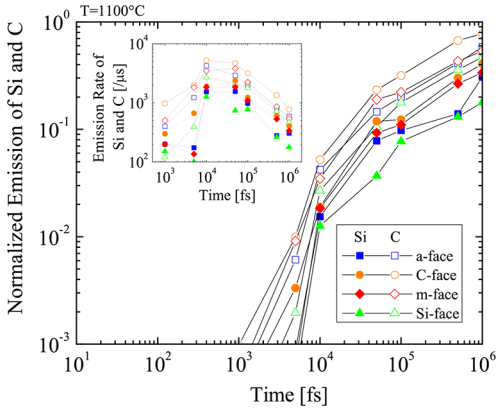

Figure 9. Time evolution of the emitted Si (closed) and C (open symbols) atoms for the a-, C-, m-, and Si-face at T = 1100 °C. The inset figure shows the emission rates of Si and C.

DOI: 10.1021/acs.jpca.7b08983
J. Phys. Chem. A 2017, 121, 8791−8798

yet require an emission of the Si and C species. On the other hand, at times >100 ps the emission is considerably decelerated due to the formation of the SiO_2 layer. However, the oxidation rate appears not to be limited by the diffusion of the Si and C interstitials but is limited by the reaction of the surface oxidation.

To investigate the orientation-dependent oxidation further, we have calculated the growth rates of SiC oxidation $(dX(SiO_2)/dt)$[46] at $t = 10^1$, 10^2, 10^3, 10^4, 10^5, and 10^6 fs, as shown in Figure 10. It is evident, that the oxidation rate

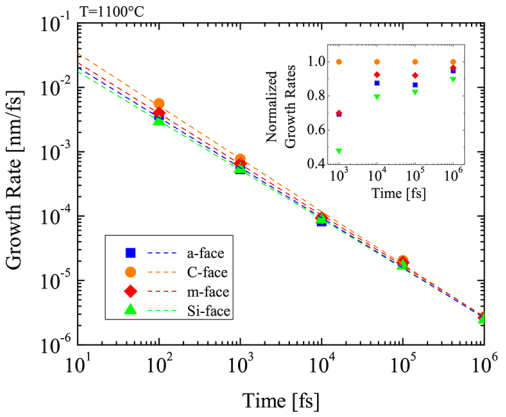

Figure 10. Time evolution of the oxidation growth rate for the a-, C-, m-, and Si-face at $T = 1100$ °C. The dashed lines are best linear fits of the log−log figure to guide the eye. The inset figure shows normalized growth rates according to the SiC orientation.

decreases exponentially with time. In fact, the growth rates are extremely high at the beginning, when the oxide layer has not been formed yet due to the absence of rate-limiting barriers, such as e.g. substantial mass transport. Therefore, the rates are comparable with the relative movement of the O_2 molecules in air. The orientation dependence of the SiC oxidation is evident during the entire simulation. In particular, the C-face has by far the highest growth rate, followed by the m- and a-face and finally the Si-face with the lowest oxidation rate. This sequence is consistent with the present macroscopic models[9,11,22] and the findings of experiments.[19,47,48] Normalized growth rates show that the orientation dependence is highest at the beginning and decreases with the grown oxide. This implies that the passivation of the oxidation mechanism due to the in-diffusion of O_2 and out-diffusion of product gases through the grown oxide layer is not orientation-dependent. Goto et al.[9] suggested that the growth rates of the surface oxidation of SiC correspond to the number of Si−C broken bonds, i.e., one Si−C back-bond for the C-face, two Si−C back-bonds for the a-face, and three Si−C back-bonds for the Si-face, yielding growth rate ratios of C-:a-:Si-face close to 1:2:3. The results for the different crystal structures from our simulations in Figure 3 are in agreement with suggestions from the macroscopic modeling. Referring back to Figures 6 and 7, we observe equivalent ratios between the three faces. On the other hand, the reason for the growth rates of m-face being 5−10% higher than of the a-face is still not fully known and should be investigated further. Homoepitaxial layers of m-face SiC are currently not available; therefore, experimental findings, to compare simulation results with, are not available.

In addition, we have calculated growth rates as a function of the oxide thicknesses for $T = 900$, 1000, 1100, and 1200 °C, shown in Figure 11. The results show that the growth rates below 3 nm are extremely high and decrease exponentially. The slopes of the curves do not decrease, which, according to the Si and C emission theory,[14] suggests that for the whole time of our simulations the surface oxidation is the rate-limiting step rather than the interface oxidation or diffusion. Note that for thin oxides (<10 nm) the rate-limiting step cannot be exactly determined. Unfortunately, we were not able to compare the results to macroscopic models,[9,14,22] as these investigate thicknesses >10 nm, which is not feasible with current simulation capabilities due to the required simulation times in the regime of several months.

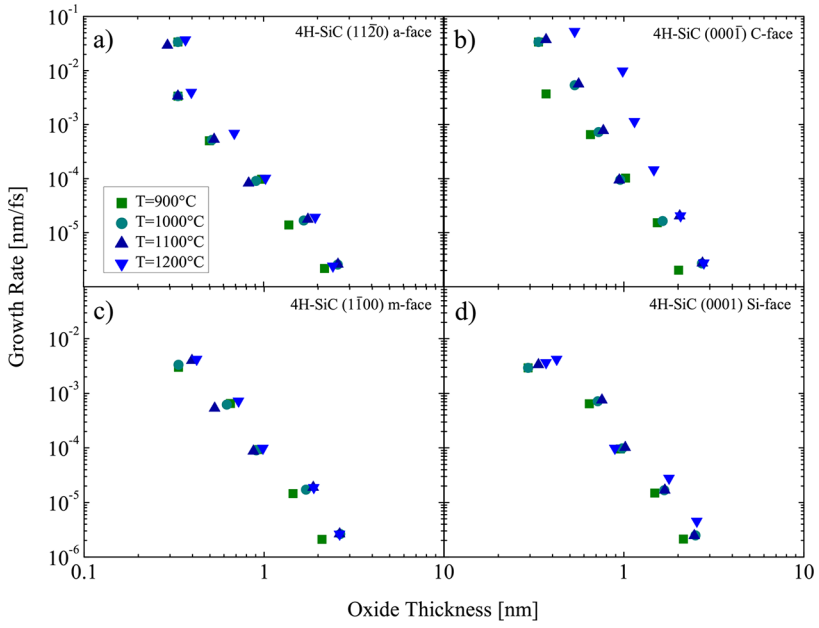

Figure 11. Growth rate of the oxidation process as a function of the oxide thickness for the (a) a-, (b) C-, (c) m-, and (d) Si-face. Colors refer to various oxidation temperatures in the range from 900 to 1200 °C.

DOI: 10.1021/acs.jpca.7b08983
J. Phys. Chem. A 2017, 121, 8791−8798

CONCLUSIONS

We have performed numerous reactive force field (ReaxFF) molecular dynamics simulations of SiC oxidation with respect to various crystallographic faces, i.e., a $(11\bar{2}0)$, C $(000\bar{1})$, m $(1\bar{1}00)$, and Si (0001), investigating the critical orientation dependence in the early stage of the oxidation process. The time evolution of the Si, C, and O atoms incorporated into the crystal structure has been extracted and analyzed for the considered oxidation temperatures ranging from 900 to 1200 °C. Oxide thicknesses have been accurately determined from the simulation results showing that even in the early stage of the SiC oxidation (up to 1 ns) an orientation dependence is evident. The oxide thickness after 2×10^6 time steps of 0.5 fs has been found to be approximately 2.5 nm. The comparison between the emitted Si and C species from the SiC crystal has shown a 3 times higher emission of the C interstitials. An unexpected maximum has been observed for the time evolution of the Si and C emission rates between 10^4 and 10^5 fs. Emissions of Si and C have been observed to be orientation-dependent as well. The calculated growth rates have indicated that the C-face has the highest oxidation rate, followed by the m-, a-, and Si-face. Furthermore, the differences in growth rates between the various faces have been observed to be decreasing with time.

This study contributes to the development of orientation-dependent SiC oxidation models,[10] which are fundamental for device fabrication simulators, e.g., Silvaco's Victory Process simulator.[49] It is crucial for device fabrication to accurately predict oxidation growth of SiC incorporating the geometry of the oxide in modern electron devices, which require intricate oxide geometries. In addition, our study promotes the advancement of the theory of SiC oxidation. As an outlook, investigations of various oxidation atmospheres, e.g., nitric oxide (NO), are of further interest due to a potentially reduced trap density in SiO_2 and other (yet unknown) effects. To sum up, a deeper fundamental understanding of the oxidation mechanisms enables performance improvements of emerging SiC-based devices.

ASSOCIATED CONTENT

Supporting Information

The Supporting Information is available free of charge on the ACS Publications website at DOI: 10.1021/acs.jpca.7b08983.

LAMMPS files (ZIP)

AUTHOR INFORMATION

Corresponding Author

*E-mail: weinbub@iue.tuwien.ac.at (J.W.).

ORCID

Josef Weinbub: 0000-0001-5969-1932

Notes

The authors declare no competing financial interest.

ACKNOWLEDGMENTS

The financial support by the Austrian Federal Ministry of Science, Research and Economy and the National Foundation for Research, Technology and Development is gratefully acknowledged. The computational results presented have been achieved using the Vienna Scientific Cluster (VSC).

REFERENCES

(1) Choyke, W. J.; Matsunami, H.; Pensl, G. *Silicon Carbide: Recent Major Advances*; Springer Science & Business Media: 2013.

(2) Kimoto, T.; Cooper, J. A. *Fundamentals of Silicon Carbide Technology: Growth, Characterization, Devices and Applications*; John Wiley & Sons: Singapore, 2014.

(3) Liu, G.; Tuttle, B. R.; Dhar, S. Silicon Carbide: A Unique Platform for Metal-Oxide-Semiconductor Physics. *Appl. Phys. Rev.* **2015**, *2*, 021307.

(4) Owens, W.; Merkel, D.; Sansoz, F.; Fletcher, D. Fracture Behavior of Woven Silicon Carbide Fibers Exposed to High-Temperature Nitrogen and Oxygen Plasmas. *J. Am. Ceram. Soc.* **2015**, *98*, 4003−4009.

(5) Opila, E. Integrated High Payoff Rocket Propulsion Technology (IHPRPT) SiC Recession Model, 2009.

(6) Nipoti, R.; Parisini, A.; Sozzi, G.; Puzzanghera, M.; Parisini, A.; Carnera, A. Structural and Functional Characterizations of Al^+ Implanted 4H-SiC Layers and Al^+ Implanted 4H-SiC pn Junctions after 1950°C Post Implantation Annealing. *ECS J. Solid State Sci. Technol.* **2016**, *5*, P621−P626.

(7) Šimonka, V.; Hössinger, A.; Weinbub, J.; Selberherr, S. Empirical Model for Electrical Activation of Aluminium and Boron Doped Silicon Carbide. *IEEE Trans. Electron Devices* **2017**, in review.

(8) Knaup, J. M.; Deák, P.; Frauenheim, T.; Gali, A.; Hajnal, Z.; Choyke, W. J. Theoretical Study of the Mechanism of Dry Oxidation of 4H-SiC. *Phys. Rev. B: Condens. Matter Mater. Phys.* **2005**, *71*, 235321.

(9) Goto, D.; Hijikata, Y.; Yagi, S.; Yaguchi, H. Differences in SiC Thermal Oxidation Process Between Crystalline Surface Orientations Observed by In-Situ Spectroscopic Ellipsometry. *J. Appl. Phys.* **2015**, *117*, 095306.

(10) Šimonka, V.; Nawratil, G.; Hössinger, A.; Weinbub, J.; Selberherr, S. Anisotropic Interpolation Method of Silicon Carbide Oxidation Growth Rates for Three-Dimensional Simulation. *Solid-State Electron.* **2017**, *128*, 135−140.

(11) Šimonka, V.; Hössinger, A.; Weinbub, J.; Selberherr, S. Growth Rates of Dry Thermal Oxidation of 4H-Silicon Carbide. *J. Appl. Phys.* **2016**, *120*, 135705.

(12) Palmour, J.; Cheng, L.; Pala, V.; Brunt, E.; Lichtenwalner, D.; Wang, G.-Y.; Richmond, J.; O'Loughlin, M.; Ryu, S.; Allen, S. et al. Silicon Carbide Power MOSFETs: Breakthrough Performance from 900 V up to 15 kV. Proceedings of Power Semiconductor Devices & IC's, 2014; pp 79−82; DOI: 10.1109/ispsd.2014.6855980.

(13) Lelis, A. J.; Green, R.; Habersat, D. B.; El, M. Basic Mechanisms of Threshold-Voltage Instability and Implications for Reliability Testing of SiC MOSFETs. *IEEE Trans. Electron Devices* **2015**, *62*, 316−323.

(14) Goto, D.; Hijikata, Y. Unified Theory of Silicon Carbide Oxidation Based on the Si and C Emission Model. *J. Phys. D: Appl. Phys.* **2016**, *49*, 225103.

(15) Heidel, T. D.; Henshall, D.; Gradzki, P. Strategies for Wide Bandgap, Inexpensive Transistors for Controlling High-Efficiency Systems. CS MANTECH Techical Digest, 2015; pp 1−4.

(16) Hijikata, Y. *Physics and Technology of Silicon Carbide Devices*; InTech: Rijeka, Croatia, 2013; DOI: 10.5772/3428.

(17) Schürmann, M.; Dreiner, S.; Berges, U.; Westphal, C. Structure of the Interface Between Ultrathin SiO 2 Films and 4H-SiC (0001). *Phys. Rev. B: Condens. Matter Mater. Phys.* **2006**, *74*, 035309.

(18) Fiorenza, P.; Raineri, V. Reliability of Thermally Oxidized SiO_2/4H-SiC by Conductive Atomic Force Microscopy. *Appl. Phys. Lett.* **2006**, *88*, 212112.

(19) Ahn, J. J.; Jo, Y. D.; Kim, S. C.; Lee, J. H.; Koo, S. M. Crystallographic Plane-Orientation Dependent Atomic Force Microscopy-Based Local Oxidation of Silicon Carbide. *Nanoscale Res. Lett.* **2011**, *6*, 235.

(20) Harris, C.; Afanas'ev, V. SiO_2 as an Insulator for SiC Devices. *Microelectron. Eng.* **1997**, *36*, 167−174.

(21) Deal, B. E.; Grove, A. General Relationship for the Thermal Oxidation of Silicon. *J. Appl. Phys.* **1965**, *36*, 3770−3778.

DOI: 10.1021/acs.jpca.7b08983
J. Phys. Chem. A 2017, 121, 8791−8798

(22) Song, Y.; Dhar, S.; Feldman, L. C.; Chung, G.; Williams, J. R. Modified Deal Grove Model for the Thermal Oxidation of Silicon Carbide. *J. Appl. Phys.* **2004**, *95*, 4953−4957.
(23) Massoud, H. Z.; Plummer, J. D.; Irene, E. A. Thermal Oxidation of Silicon in Dry Oxygen Growth-Rate Enhancement in the Thin Regime I. Experimental Results. *J. Electrochem. Soc.* **1985**, *132*, 2685−2693.
(24) Massoud, H. Z.; Plummer, J. D.; Irene, E. A. Thermal Oxidation of Silicon in Dry Oxygen: Growth-Rate Enhancement in the Thin Regime II. Physical Mechanisms. *J. Electrochem. Soc.* **1985**, *132*, 2693−2700.
(25) Yamamoto, T.; Hijikata, Y.; Yaguchi, H.; Yoshida, S. Oxide Growth Rate Enhancement of Silicon Carbide (0001) Si-faces in Thin Oxide Regime. *Jpn. J. Appl. Phys.* **2008**, *47*, 7803.
(26) Yamamoto, T.; Hijikata, Y.; Yaguchi, H.; Yoshida, S. Oxygen-Partial-Pressure Dependence of SiC Oxidation Rate Studied by In Situ Spectroscopic Ellipsometry. Proceedings of Materials Science Forum, 2009; pp 667−670; DOI: 10.4028/www.scientific.net/msf.600-603.667.
(27) Yamamoto, T.; Hijikata, Y.; Yaguchi, H.; Yoshida, S. Growth Rate Enhancement of (0001)-Face Silicon-Carbide Oxidation in Thin Oxide Regime. *Jpn. J. Appl. Phys.* **2007**, *46*, L770.
(28) Hijikata, Y.; Yaguchi, H.; Yoshida, S. A Kinetic Model of Silicon Carbide Oxidation Based on the Interfacial Silicon and Carbon Emission Phenomenon. *Appl. Phys. Express* **2009**, *2*, 021203.
(29) Hijikata, Y.; Yaguchi, H.; Yoshida, S. Theoretical Studies for Si and C Emission Into SiC Layer During Oxidation. Proceedings of Materials Science Forum, 2011; pp 429−432; DOI: 10.4028/www.scientific.net/msf.679-680.429.
(30) Kageshima, H.; Shiraishi, K.; Uematsu, M. Universal Theory of Si Oxidation Rate and Importance of Interfacial Si Emission. *Jpn. J. Appl. Phys.* **1999**, *38*, L971.
(31) Newsome, D. A.; Sengupta, D.; Foroutan, H.; Russo, M. F.; van Duin, A. C. Oxidation of Silicon Carbide by O2 and H_2O: A ReaxFF Reactive Molecular Dynamics Study, Part I. *J. Phys. Chem. C* **2012**, *116*, 16111−16121.
(32) Ciccotti, G.; Ferrario, M.; Schuette, C. Molecular Dynamics Simulation. *Entropy* **2014**, *16*, 233.
(33) Van Duin, A. C.; Dasgupta, S.; Lorant, F.; Goddard, W. A. ReaxFF: A Reactive Force Field for Hydrocarbons. *J. Phys. Chem. A* **2001**, *105*, 9396−9409.
(34) Senftle, T. P.; Hong, S.; Islam, M. M.; Kylasa, S. B.; Zheng, Y.; Shin, Y. K.; Junkermeier, C.; Engel-Herbert, R.; Janik, M. J.; Aktulga, H. M.; et al. The ReaxFF Reactive Force-Field: Development, Applications and Future Directions. *npj Computational Materials* **2016**, *2*, 15011.
(35) Li, G.-Y.; Ding, J.-X.; Zhang, H.; Hou, C.-X.; Wang, F.; Li, Y.-Y.; Liang, Y.-H. ReaxFF Simulations of Hydrothermal Treatment of Lignite and its Impact on Chemical Structures. *Fuel* **2015**, *154*, 243−251.
(36) Han, S.; Li, X.; Nie, F.; Zheng, M.; Liu, X.; Guo, L. Revealing the Initial Chemistry of Soot Nanoparticle Formation by ReaxFF Molecular Dynamics Simulations. *Energy Fuels* **2017**, *31*, 8434−8444.
(37) Islam, M. M.; Ostadhossein, A.; Borodin, O.; Yeates, A. T.; Tipton, W. W.; Hennig, R. G.; Kumar, N.; van Duin, A. C. ReaxFF Molecular Dynamics Simulations on Lithiated Sulfur Cathode Materials. *Phys. Chem. Chem. Phys.* **2015**, *17*, 3383−3393.
(38) Han, S. S.; Choi, S.-H.; van Duin, A. C. Molecular Dynamics Simulations of Stability of Metal-Organic Frameworks Against H_2O Using the ReaxFF Reactive Force Field. *Chem. Commun.* **2010**, *46*, 5713−5715.
(39) Kulkarni, A. D.; Truhlar, D. G.; Goverapet Srinivasan, S.; van Duin, A. C.; Norman, P.; Schwartzentruber, T. E. Oxygen Interactions with Silica Surfaces: Coupled Cluster and Density Functional Investigation and the Development of a new ReaxFF Potential. *J. Phys. Chem. C* **2013**, *117*, 258−269.
(40) Fogarty, J. C.; Aktulga, H. M.; Grama, A. Y.; Van Duin, A. C.; Pandit, S. A. A Reactive Molecular Dynamics Simulation of the Silica-Water Interface. *J. Chem. Phys.* **2010**, *132*, 174704.
(41) Kylasa, S. B.; Aktulga, H. M.; Grama, A. PuReMD-GPU: A Reactive Molecular Dynamics Simulation Package for GPUs. *J. Comput. Phys.* **2014**, *272*, 343−359.
(42) Aktulga, H. M.; Fogarty, J. C.; Pandit, S. A.; Grama, A. Y. Parallel Reactive Molecular Dynamics: Numerical Methods and Algorithmic Techniques. *Parallel Computing* **2012**, *38*, 245−259.
(43) Seyller, T. Passivation of Hexagonal SiC Surfaces by Hydrogen Termination. *J. Phys.: Condens. Matter* **2004**, *16*, S1755.
(44) Berendsen, H.; Postma, J.; van Gunsteren, W.; DiNola, A.; Haak, J. Molecular Dynamics with Coupling to an External Bath. *J. Chem. Phys.* **1984**, *81*, 3684.
(45) Vienna Scientific Cluster; http://vsc.ac.at/ (accessed October 19, 2017).
(46) Newsome, D. A.; Sengupta, D.; van Duin, A. C. High-Temperature Oxidation of SiC-Based Composite: Rate Constant Calculation from ReaxFF MD Simulations, Part II. *J. Phys. Chem. C* **2013**, *117*, 5014−5027.
(47) Gupta, S. K.; Akhtar, J. *Thermal Oxidation of Silicon Carbide (SiC)-Experimentally Observed Facts*; INTECH: 2011; DOI: 10.5772/20465.
(48) Kakubari, K.; Kuboki, R.; Hijikata, Y.; Yaguchi, H.; Yoshida, S. Real Time Observation of SiC Oxidation Using an In Situ Ellipsometer. Proceedings of Materials Science Forum, 2006; pp 1031−1034; DOI: 10.4028/0-87849-425-1.1031.
(49) Silvaco's Victory Process simulator; http://www.silvaco.com/products/tcad/ (accessed October 19, 2017).

DOI: 10.1021/acs.jpca.7b08983
J. Phys. Chem. A 2017, 121, 8791−8798